Civil Engineering Infrastructures Journal xx,xx

DOI: 10.22059/ceij.2026.405512.2425

Inerter-based active tuned mass damper for mitigating wind-induced vibrations in tall TV towers

#	Name	Email Address	Degree	Position	Country	Affiliation
1	Khodaie, Nahmat	nahmat.khodaie@gmail.com	Ph.D.	Assistant Professor	Iran	Department of civil engineering, Islamic azad university, Khormouj branch, Iran

Received: 03/11/2025

Revised: 06/01/2026

Accepted: 12/02/2026

Abstract

This study evaluated the effectiveness of the inerter-based active tuned mass damper (ATMDI) for controlling wind-induced vibrations in tall TV towers, and compared its performance with other systems, including the traditional tuned mass damper (TMD), tuned mass damper with an inerter (TMDI), and active tuned mass damper (ATMD). A multi-degree-of-freedom model of a tall TV tower was analyzed using the frequency-domain method for various wind speeds, in both crosswind and along-wind directions. The results indicated that crosswind vibrations

exceeded along-wind vibrations, with crosswind acceleration surpassing human comfort limits for the uncontrolled structure. The performance of these systems in reducing crosswind acceleration was examined parametrically, considering key variables such as damper mass ratio, inertance ratio, and ATMDI optimization parameters. The advantages and limitations of the studied systems were also discussed. While all systems reduced crosswind acceleration, the ATMDI demonstrated the most significant improvement, benefiting from both the active control mechanism and the mass amplification effect provided by the inerter. Additionally, the inerter reduced the damper stroke compared to the ATMD, addressing a key limitation of the latter.

Key words: wind-induced vibration, TV tower, vibration control, active control, inerter

1. Introduction

With the advancement of progressively taller and more intricate civil structures, concerns have arisen regarding their safety during natural disasters, such as earthquakes and typhoons. Due to the low inherent damping and high aspect ratio of tall TV towers, these structures are vulnerable to wind dynamic loads in both the along-wind and crosswind directions. Occupant discomfort due to wind-induced vibrations is a major serviceability concern in the design of tall and slender structures (Ubertini et al., 2017). Users' comfort to vibrations is evaluated based on the acceleration at the level of interest, which is usually the highest occupied floor (Johann et al., 2015). Typical acceptable ranges for peak accelerations, based on a 10-year Mean Return Interval (MRI), are 0.15–0.20 m/s² for office buildings and 0.10–0.15 m/s² for residential buildings (Simiu, 2011; Simiu and Yeo, 2019).

In recent years, the application of structural control strategies to mitigate the vibrations of tall structures has received increasing attention, with a focus on enhancing their safety and

performance (Wani et al., 2022). Passive control methods, such as tuned-mass and tuned-liquid dampers, are cost-effective and straightforward to apply. They have been extensively studied for vibration control. Zhang et al. (2009) examined fluid-viscous dampers to mitigate along-wind vibrations in the Hefei TV tower. Najafi et al (2024) conducted an eexperimental and numerical study to examine the performance of friction damper on the seismic behavior of RC bending frames. Cetin et al. (2025) experimentally investigated a TMD on a 10-story steel frame under harmonic and seismic excitations. The results demonstrated the TMD's high effectiveness in reducing structural displacements and accelerations, confirming its potential as a passive control solution for enhancing seismic resilience. Khodaie and Eimani (2018) proposed a self-control approach to suppress vibrations caused by wind loads in tall TV towers. Khodaie (2020) investigated the effect of integrating the tapering strategy as an aerodynamic modification and TMD system to control wind effects in super-tall buildings. Aydin et al. (2023) experimentally studied different pendulum damper placements on a 3-storey frame under harmonic excitations. They concluded that dampers were highly effective at structural resonance, and models with multiple dampers also reduced dynamic response. Suthar and Jangid (2021) proposed an optimal design methodology for tuned liquid sloshing dampers to control across-wind response in tall buildings. Cetin et al. (2025) presented an optimization procedure for Multiple Tuned Mass Dampers (MTMDs) to control vibrations in cantilever beams under harmonic, seismic, and wind excitations. Their optimized system indicated significant reductions in displacement, acceleration, and rotational responses of the beam. Similar optimization and efficacy of MTMDs have also been investigated for vibration control in tall structures (Elias et al., 2019 and Yang et al., 2021).

Recent studies have explored advanced control strategies, such as integrating TMDs with active or semi-active systems (Pinkaew et al., 2001 and Li et al., 2011). Kim et al. (2014)

investigated ATMD systems, which showed significant improvements in vibration control. He and Li (2014) studied the motion data of a 492-meter-high building equipped with an ATMD, during a typhoon event. Shahi et al. (2018) examined seismic control of high-rise buildings using ATMDs, accounting for soil-structure interaction effects. Zhou et al. (2020) examined vibrations in a high-rise building equipped with a 600-ton ATMD system during a super typhoon, using an LQR-based control algorithm. Jafari and Alipour (2021) reviewed methods for controlling wind-induced vibrations in tall buildings, emphasizing both passive and active strategies, and highlighted the effectiveness of damping systems and aerodynamic modifications.

The inerter device, introduced by Smith (2002), has been extensively studied over the past two decades to enhance conventional passive control systems. This two-dimensional mechanical element generates a force that is proportional to the relative acceleration between its terminals (Ma et al., 2021). Essentially, an inerter mimics a system with high inertia but has a very small mass (Wu et al., 2022). When combined with TMDs, various tuned mass-damper-inerter (TMDI) configurations can be designed, either by replacing the TMD mass or increasing its inertial effect (Weber et al., 2022). Research on TMDI has shown its effectiveness in suppressing seismic excitations (Lazar et al., 2014; Lara-Valencia et al., 2020; Wu et al., 2022), with the advantage of achieving better vibration control with less added mass compared to TMDs. Su et al. (2022) examined inerter-based double tuned mass dampers to improve wind-induced vibration control and reduce weight in slender structures. Qiao et al. (2022) studied structural control of high-rise buildings using TMDI under multi-hazard excitations, optimizing design parameters for wind and earthquake responses. Suthar and Banerji (2023) introduce an inerter-assisted pendulum-tuned mass damper for crosswind response control in tall buildings. De Angelis et al. (2023) investigated the optimal design and placement of TMDI in MDOF

structures for enhanced performance. Suthar (2024) proposes an inerter-assisted tuned liquid sloshing damper (IA-TLSD) for vibration control in SDOF systems, enhancing performance over traditional TLSDs. Pen and Sun (2024) performed reliability-based design optimization of TMDI to mitigate structural vibration, improving control and reducing mass. Similar studies have also explored the mitigation of wind-induced oscillations in tall buildings using TMDI (Giaralis and Petrini, 2017a,b; Zhang and Fitzgerald, 2020). Furthermore, TMDI systems have been investigated for controlling vibrations in bridges subjected to earthquakes and wind loads (Xu et al., 2019; Dai et al., 2019, 2021; Liang et al., 2021). Additionally, Wang et al. (2020) and Pandey et al. (2021) examined the use of inerters to enhance the performance of tuned liquid column dampers.

Previous studies have focused on the role of inerters in passive control systems. This study explores the use of an inerter in combination with active mass dampers to control wind-induced vibrations in tall TV towers. A numerical example of a tall TV tower is presented, modeled as a multi-degree-of-freedom (MDOF) cantilever beam with lumped masses. The wind-induced responses are computed and compared under various conditions, including an uncontrolled structure, structures equipped with TMDs (with and without an inerter), and structures with ATMDs (with and without an inerter). The study also examines the effects of various parameters, such as basic wind speed, inertance ratio, TMD mass ratio, and ATMD system parameters, through a parametric analysis.

2. Wind effects

2.1. Mean wind speed profile

In this study, the power law is utilized for the wind velocity profile, as expressed below (Kwon and Kareem, 2013):

$$U(z) = aU_b(\frac{z}{b})^{\alpha} \tag{1}$$

where U_b denotes the basic wind speed, a, b, and α are terrain constants, and z represents height.

2.2. Along-wind loads

Along-wind force is stated as the sum of a mean and a fluctuating part. The mean component $\bar{f}_D$ and the dynamic component $f'_D(t)$ per unit height are specified as follows (Simiu, 2011):

$$\bar{f}_D = \frac{1}{2}\rho_a \bar{U}^2 C_D B\,, \quad f'_D(t) = \rho_a \bar{U} u(t) C_D B \tag{2}$$

where ρ_a represents air density, $\bar{U}$ is the mean wind velocity, *u(t)* is the along-wind fluctuating speed, C_D denotes the drag coefficient, and B represents the length perpendicular to the wind direction. The power spectral density (PSD) of the along-wind dynamic force is:

$$S_{f_D}(\omega) = \rho_a^2 \bar{U}^2 B^2 {C_D}^2 S_u(\omega) \tag{3}$$

where $S_u(\omega)$ is PSD of the fluctuating wind speed, which can be obtained using the following formula (Simiu, 2011):

$$S_u(z,n) = \frac{{u_*}^2}{n}\frac{200f}{[1+50f]^{5/3}} \qquad f = \frac{nz}{\bar{U}(z)} \tag{4}$$

where z, u_* and $\bar{U}(z)$ denote altitude, friction velocity, and mean velocity at the point considered, respectively, and $f = \frac{nz}{\bar{U}(z)}$ is the reduced frequency. The wind speed correlation between two distinct points can be computed using the following relation (Simiu, 2011):

$$coh_{jk}(n,z) = exp\left(-\frac{nc_z\left|(z_j - z_k)\right|}{1/2[\bar{U}(z_j) + \bar{U}(z_j)]}\right) \tag{5}$$

The recommended value for the constant c_z is 10.

2.3. Cross-wind loads

The PSD of the crosswind force can be expressed as follows (Simiu, 2011):

$$S_{F_s}(z,n)=\left[\frac{1}{2}\rho_a D(z)U^2(z)\right]^2 S_{C_L}(z,n) \tag{6}$$

where $S_{C_L}(z,n)$ is the lift coefficient spectrum:

$$\frac{S_{C_L}(z,n)}{\bar{C}_L^2}=\frac{1}{\sqrt{\pi}Bn_s}\left[-\left(\frac{1-(\frac{n}{n_s})}{B}\right)^2\right] \tag{7}$$

where n denotes frequency, $\bar{C}_L$ represents the root-mean-square (RMS) lift coefficient, and n_s corresponds to the shedding frequency, around which the fluctuating lift force is focused:

$$n_s=\frac{S_t U(z)}{D(z)} \tag{8}$$

S_t is the Strouhal number. B represents bandwidth, which is an indicator of the breadth of the lift spectrum:

$$B^2=B_0^2+2I_z^2 \tag{9}$$

B_0 denotes smooth flow bandwidth, which typically ranges from 0.05 to 0.1, and I_z is the turbulence intensity. The lift coefficient $\bar{C}_L$, Strouhal number S_t, and the aerodynamic damping in the vortex-induced-vibration (VIV) lock-in range ζ_a were obtained using the following formulas (Menon and Rao, 1997):

$$\bar{C}_L=[0.46+0.07\,log(K_s/\bar{D})](0.754log(H/\bar{D})-0.074) \tag{10}$$

$$S_t=[0.175-0.015log(K_s/\bar{D})](0.452log(H/\bar{D})+0.348) \tag{11}$$

$$\zeta_a=-\left(\frac{\rho_a\bar{D}^2}{m_{eq}}\right)K_a \quad , \quad K_a=K_{a0}\left(1-\left(\frac{\sigma_y}{\sigma_{y_L}}\right)\right) \tag{12}$$

$$K_{a0}=[0.87+0.08\,log(K_s/\bar{D})](0.754log(H/\bar{D})-0.074)$$

where H is height, $\bar{D}$ is the effective diameter, which is equal to the averaged diameter over the top one-third of the structure, K_s is the equivalent sand roughness, σ_y is the RMS tip

displacement, $\sigma_{y_L} = 0.4\overline{D}$ is a limiting RMS displacement, and m_{eq} is the equivalent mass obtained as:

$$m_{eq} = \frac{\int_0^H m(z)\varphi_r{}^2(z)dz}{\int_0^H \varphi_r{}^2(z)dz} \tag{13}$$

where $\varphi_r(z)$ is the mode shape, and $m(z)$ is the vibrating mass per unit length.

The coherence function between the crosswind forces at two different heights is obtained using the following equation (Simiu, 2011):

$$coh_{jk} = cos(2r/3)\, exp(-(r/3)^2), \quad r = \frac{2|z_j - z_k|}{D(z_j) + D(z_k)} \tag{14}$$

3. Analytical model

3.1. Structure dynamic properties

The equation governing the vibration of MDOF structures under dynamic excitations can be expressed as follows:

$$\boldsymbol{M_s\ddot{X} + C_s\dot{X} + K_sX = F} \tag{15}$$

where X represents the nodal displacements vector and F denotes the vector of excitation forces. K_s, C_s, and M_s stand for stiffness, damping and mass matrices, respectively. The procedure for determining these matrices for the specific structural model can be found in prior studies (Khodaie and Eimani, 2018; Khodaie, 2020).

3.2. Modeling of TMD and Inerter systems

General representation of a rack and pinion-type inerter is shown in Fig. 1(a). The inerter force (Fig. 1(b)) can be written as follows:

$$f_b = b(\ddot{u}_2 - \ddot{u}_1) \tag{16}$$

where b denotes inertance, and $\ddot{u}$ represents acceleration response at the inerter terminals. Fig. 2 illustrates the schematic of the studied tower and its analytical model equipped with the TMDI and ATMDI systems, along with a conceptual detail for the installation of the inerter. In this configuration, one terminal is connected to the mass damper, while the other terminal is attached at a lower height to the internal wall of the tower shaft.

Since the inerter force is proportional to the relative acceleration between its terminals, the mass amplification effect of the inerter on the TMDI system is significant when one of its terminals is connected to the ground or a structural point with a lower acceleration response (Ma et al., 2021). Therefore, this approach is adopted in the present research, where the inerter is connected between the TMD and the *i*-th node of the structure, which is at a lower height than the TMD (Fig. 2(b)).

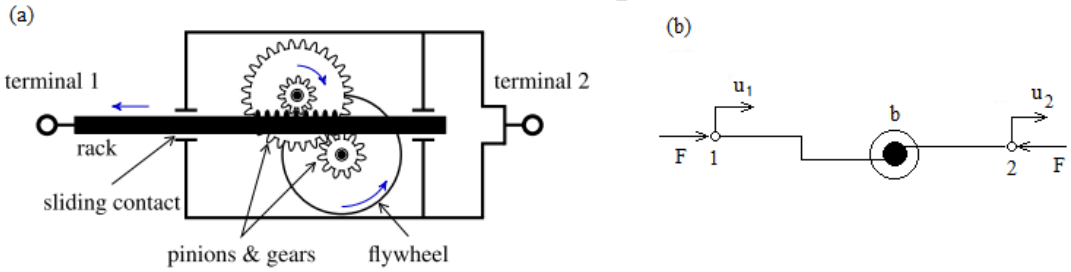

Fig. 1 Scheme of: (a) rack and pinion-type inerter (Sun et al., 2017) (b) an inerter with associated DOFs (Pandey DK, Mishra, 2021)

The equation of motion for a TMDI-equipped structure is similar to Eq. (14), requiring the inclusion of the inerter, TMD's mass, stiffness, and damping effects into the corresponding overall matrices. For instance, the mass matrix for an MDOF structure with a TMDI system (Fig. 2(b)) is given by:

$$\boldsymbol{M} = \begin{bmatrix} m_1 & 0 & & 0 & & 0 & 0 \\ 0 & m_2 & & 0 & & 0 & 0 \\ \vdots & \vdots & & \vdots & & \vdots & \vdots \\ 0 & 0 & \cdots & m_i + b & \ldots & 0 & -b \\ \vdots & \vdots & & \vdots & & \vdots & \vdots \\ 0 & 0 & & 0 & & m_n & 0 \\ 0 & 0 & & -b & & 0 & m_{TMDI} + b \end{bmatrix} \tag{17}$$

$$m_{TMDI} = \mu M_1, \qquad b = \beta M_1 \tag{18}$$

where n is the number of the lumped masses of the structure, μ is the TMDI's mass ratio, β is the inertance ratio, and M_1 is the first modal mass of the structure. When the inertance ratio β is zero, the TMDI system becomes equivalent to the traditional TMD system. Details of obtaining the stiffness and damping matrices for a TMD-equipped structure can be found in Khodaie (2020). The frequency and damping ratios for the TMDI system are defined as follows (Giaralis and Petrini, 2017b):

$$f_r = \frac{\sqrt{k_{TMDI}/(m_{TMDI} + b)}}{\omega_1} \qquad \zeta_r = \frac{c_{TMDI}}{2\sqrt{(m_{TMDI} + b)k_{TMDI}}} \tag{19}$$

where ω_1 is the fundamental natural frequency of the primary structure, and k_{TMDI} and c_{TMDI} are the stiffness and damping constants of the system, respectively.

3.3. ATMDI system and the state-space equations

Active control systems mitigate structural motions by applying external forces. As depicted in Fig. 2, the ATMDI system includes stiffness, damping, and inerter elements, as well as a sensor and actuator to apply the anticipated active force. For an MDOF structure equipped with an ATMDI, the vibration equation is expressed as:

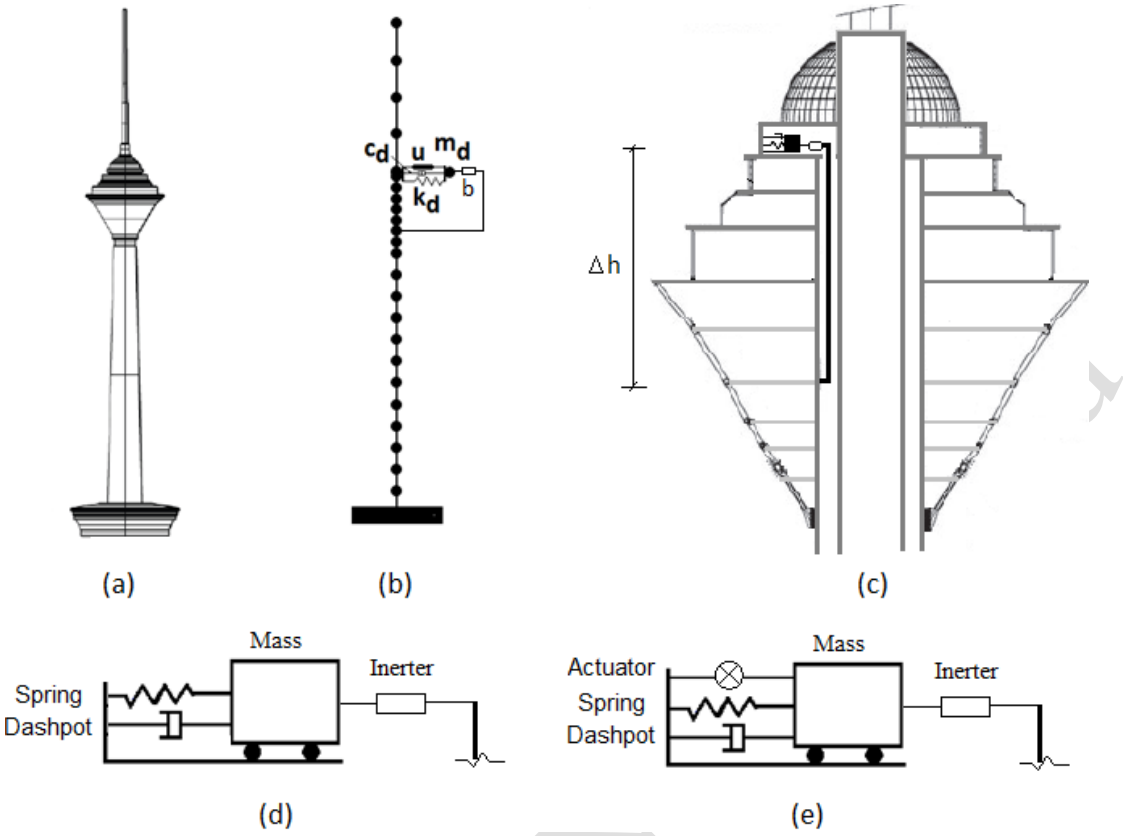

Fig. 2: (a) Schematic configuration of the studied TV tower, (b) analytical model of the structure with ATMDI, (c) schematic layout for inerter installation, and details of: (d) TMDI, and (e) ATMDI.

$$\boldsymbol{M}\ddot{\boldsymbol{X}}(t) + \boldsymbol{C}\dot{\boldsymbol{X}}(t) + \boldsymbol{K}\boldsymbol{X}(t) = \boldsymbol{B_{su}}u(t) + \boldsymbol{D_{sf}}\boldsymbol{F}(t) \tag{20}$$

where **M**, **C**, and **K** are matrices corresponding to generalized mass, damping, and stiffness, respectively, **X** and **F** are displacement and external excitation vectors, and $\boldsymbol{B_{su}}$ denotes a vector representing the position of the actuator while $\boldsymbol{D_{sf}}$ indicates the position of external forces. $\boldsymbol{B_{su}}$ and $\boldsymbol{D_{sf}}$ for the studied structure are as follows:

$$\boldsymbol{B_{su}} = \left[0_{1*(j-1)},\ \ -1,\ \ 0_{1*(n-j)},\ \ 1\right]',\quad \boldsymbol{D_{sf}} = \begin{bmatrix} I_{n*n} \\ 0_{1*n} \end{bmatrix} \tag{21}$$

where n represents the total node count in the structure and *j* signifies the specific node number where the ATMDI is installed. The state-space relations for Eq. (20) can be written as follows:

$$\dot{Z}(t) = AZ(t) + B_u u(t) + D_f F(t) \tag{22}$$

where:

$$Z(t) = \begin{bmatrix} X(t) \\ \dot{X}(t) \end{bmatrix}_{(2n+2)\times 1}, \qquad A = \begin{bmatrix} 0_{n+1} & I_{n+1} \\ -M^{-1}K & -M^{-1}C \end{bmatrix}_{(2n+2)}, \tag{23}$$

$$B_u = \begin{bmatrix} 0_{(n+1)*1} \\ M^{-1}B_{su} \end{bmatrix}_{(2n+2)\times 1}, \qquad D_f = \begin{bmatrix} 0_{(n+1)*n} \\ M^{-1}D_{sf} \end{bmatrix}_{(2n+2)\times n}$$

The structure's output can be expressed based on its current state and the applied control input. Various techniques can be employed to determine the optimal active force. The most common technique is the LQR method. Fig. 3 illustrates the application of the LQR technique to the structure under external excitations. This regulator minimizes a cost function that balances control effort and desired control performance. The cost function is given by the following performance index (Mei et al., 2020):

$$J_0 = \frac{1}{2}\int_0^{\infty} [Z^T(t)QZ(t) + u^T(t)Ru(t)]dt \tag{24}$$

where Q and R are the weight matrices for the states and input, respectively. To minimize the cost function J_o, the state equation defined by Eq. (22) serves as the constraint. Minimizing this cost function gives the relevant control force:

$$u(t) = -GZ(t) \tag{25}$$

The feedback gain matrix, G, can be obtained by solving a Riccati equation (Mei et al., 2020). In this study, as defined by Ricciardelli et al. (2003), the first term of the LQR performance index (Eq. (24)), involving the state vector, is defined as follows:

$$\begin{aligned} Z^T(t)QZ(t) = q_1 * \left({x_1}^2 + {x_2}^2 + \cdots + {x_n}^2\right) + q_2 * {x_{n+1}}^2 + \\ q_3 * \left({\dot{x}_1}^2 + {\dot{x}_2}^2 + \cdots + {\dot{x}_n}^2\right) + q_4 * {\dot{x}_{n+1}}^2 \end{aligned} \tag{26}$$

where q_1, q_2, q_3 and q_4 are variables of Q, x is the displacement, and $\dot{x}$ denotes the velocity. In the context of a narrowband response, the relationship between displacement and velocity is

nearly in phase with the angular frequency of the structure. This relationship is formally expressed by the following equation:

$$q_1/q_3 \approx q_2/q_4 \approx {\omega_1}^2 \tag{27}$$

where ω_1 represents the structure's fundamental angular frequency. Under these assumptions, the control action of the ATMDI depends on the ratios q_1/q_3 and q_1/R, which represent the relative importance of the structure's response versus the ATMDI's response and the amount of control energy consumed, respectively.

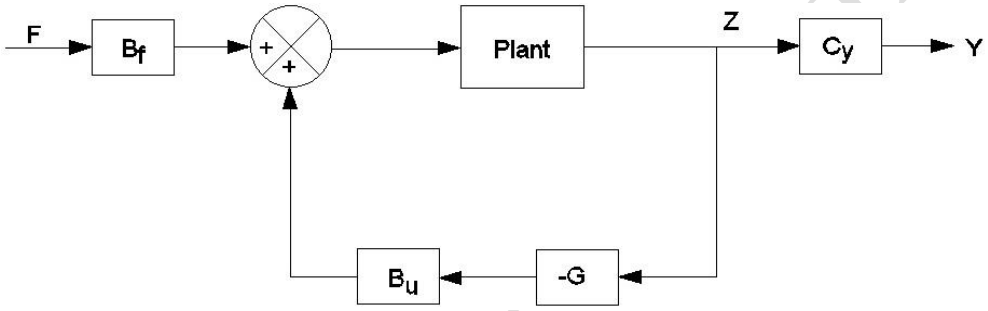

Fig. 3 Block diagram of the LQR technique applied to a structure subjected to external excitations

4. Characteristics of the tall TV tower and wind modeling assumptions

To investigate the control efficiency of the studied systems, an illustration featuring a tall TV tower is provided. The schematic layout of the examined tower is shown in Fig. 4. The assumed structure closely resembles the Milad Tower in Tehran in various structural and geometric aspects. However, since both along-wind and crosswind responses are numerically investigated in this study, which require extensive wind engineering data, and because this information is more readily available for a circular cross-section, the tower's shaft cross-section is assumed to be hollow and circular. The geometrical and physical properties of the shaft are chosen to align the natural frequency and mass of the example tower very closely with those of the Milad Tower. As illustrated in Fig. 4, the tower is constructed with three principal parts above the foundation: the shaft, head structure, and antenna mast. The shaft is a reinforced-

concrete structure, reaching a height of approximately 315 meters from the ground floor. Beginning with a 28-meter diameter at ground level, it gradually tapers to 17 meters at the 240-meter height, maintaining this diameter up to the 315-meter level. The tower's head extends from the 240-meter to the 315-meter level. Above that, there is a 120-meter-high steel antenna mast.

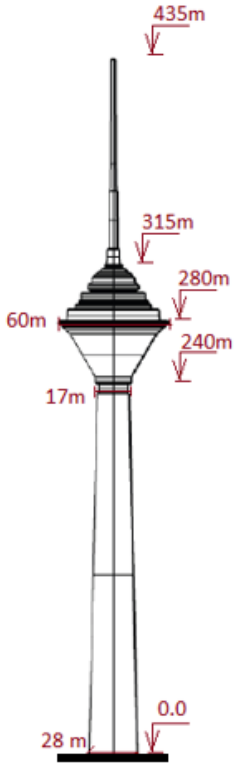

Fig. 4 Schematic configuration and dimensions of the assumed tall TV tower

As previously mentioned, the tower is regarded as an MDOF structure. A total of 25 nodes is considered. At the tower's head, due to substantial dimensional variations, the distance between the nodes is assumed to be smaller than that at other locations. Dimensional and physical characteristics of the structural model are detailed in Table 1.

The assumed values for the required parameters are as follows: ρ_a=1.25 kg/m^3, U_b=30 m/s, α=0.36, C_D=0.65 (NBCC, 2015). Additionally, the structural damping ratio is assumed to be 1.5%.

Table 1. Geometric and physical parameters characterizing the theoretical model of the tower

Node	Height(m)	Width against wind (m)	Area against wind (m^2)	Shaft outside diameter (m)	Moment of inertia (m^4)	Mass (tons)
1	20.0	27.08	541.67	27.08	11751.74	7199.53
2	40.0	26.17	523.33	26.17	9855.69	6427.60
3	60.0	25.25	505.00	25.25	8180.10	5708.71
4	80.0	24.33	486.67	24.33	6876.31	5130.86
5	100.0	23.42	468.33	23.42	5729.40	4597.52
6	120.0	22.50	450.00	22.50	4726.58	4105.64
7	140.0	21.58	431.67	21.58	3970.44	3729.56
8	160.0	20.67	413.33	20.67	3308.58	3385.86
9	180.0	19.75	395.00	19.75	2732.84	3072.35
10	200.0	18.83	376.67	18.83	2312.28	2854.03
11	220.0	17.92	358.33	17.92	1940.86	2655.75
12	240.0	17.00	270.73	17.00	1614.78	1950.41
13	250.0	27.75	277.50	17.00	1614.78	2002.28
14	260.0	38.50	385.00	17.00	1614.78	3120.98
15	270.0	49.25	492.50	17.00	1614.78	4602.74
16	280.0	60.00	567.81	17.00	1614.78	5847.98
17	290.0	45.00	456.25	17.00	1614.78	4068.04
18	300.0	35.00	350.00	17.00	1614.78	2714.86
19	310.0	25.00	189.69	17.00	1614.78	1349.87
20	314.5	17.79	52.74	17.00	1614.78	373.52
21	315.5	5.98	43.15	5.98	4.87	121.55
22	345.0	4.65	69.09	4.65	1.91	169.23
23	375.0	3.30	49.50	3.30	0.54	97.31

24	405.0	1.95	29.25	1.95	0.0834	43.45
25	435.0	0.60	7.03	0.60	0.0015	7.72

5. Analysis and Results

The structural responses are obtained for the uncontrolled structure and for structures equipped with TMD, TMDI, ATMD, and ATMDI systems. As explained later, the primary control objective for the studied tower is to reduce vibrations to levels below the human comfort threshold. According to the tower's schematic layout (Fig. 4), the highest occupancy level occurs at approximately 300 meters. This height, corresponding to node 18 and located in the upper part of the tower head, is designated as the reference height. Wind-induced responses at this level are compared across the various scenarios considered. Control efficiency is defined as the percentage reduction in the structure's response compared to the response of the uncontrolled structure. The results from the various scenarios are presented and discussed in the subsequent sections.

5.1 Uncontrolled structure

This section presents and discusses the responses of the uncontrolled tower. Fig. 5 shows the first three mode shapes of the tower. The angular frequencies associated with these modes are 0.963, 3.988, and 5.711 rad/sec. At the reference level, the static displacement is 14.48 cm for the assumed design wind speed of 30 m/s. The responses to varying basic wind speeds up to 30 m/s are computed for both along-wind and crosswind directions. Figs. 6(a) and 6(b) depict RMS displacement and acceleration at the reference height relative to the basic wind speed, respectively. As shown, along-wind responses increase parabolically with rising wind speed, while crosswind responses peak at approximately 28 m/s. This marks the critical wind speed, where the vortex shedding frequency aligns with the structure's dominant frequency. At this

speed, crosswind RMS displacement and acceleration at the reference height are 8.87 cm and 8.5 cm/s², respectively. The maximum negative crosswind aerodynamic damping ratio, corresponding to the critical wind speed, was found to be 0.39% using Eq. (12). This value is approximately 26% of the assumed structural damping ratio. The maximum along-wind responses measure 6.15 cm and 4.40 cm/s². This indicates that the crosswind acceleration and displacement are respectively 44% and 93% greater than the corresponding along-wind responses at the assumed basic wind speed.

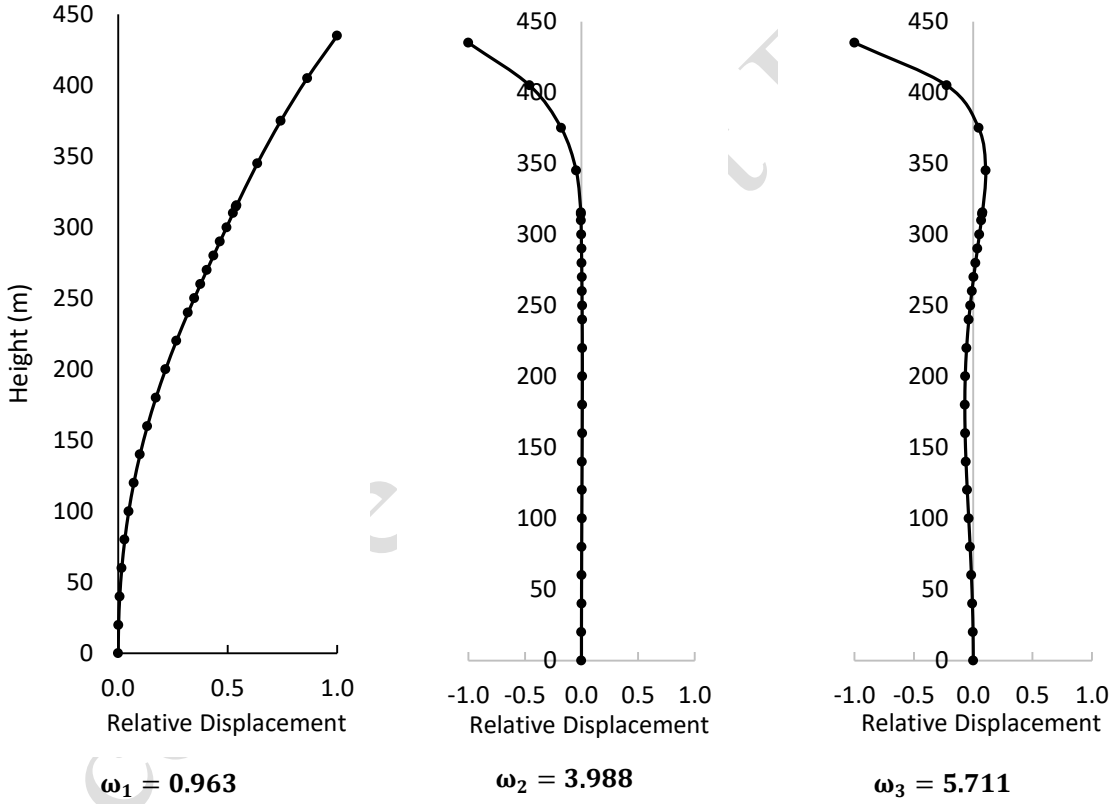

Fig. 5. The first three vibration modes and their corresponding frequencies of the tower

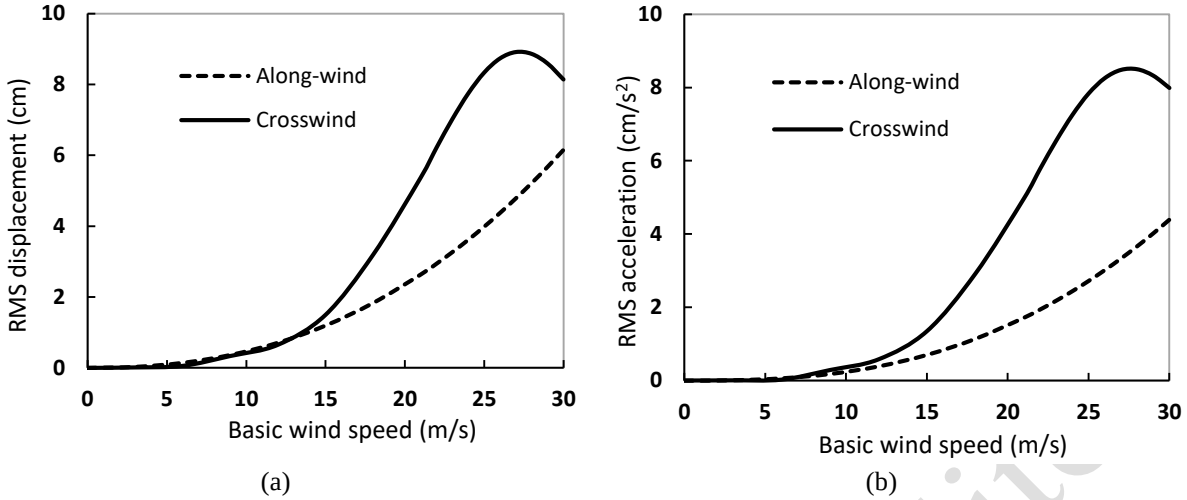

(a) (b)

Fig. 6: RMS displacement (a) and RMS acceleration (b) in the along-wind and cross-wind directions at the reference level versus basic wind speed.

The structural peak responses are determined by multiplying the RMS values by a peak factor of 3.71, derived from a relation provided by Kwon and Kareem (2013). The computed crosswind peak acceleration of 31.54 cm/s² exceeds the widely accepted comfort limit for tall structures (typically less than 20 cm/s², Simiu, 2011). Due to the dominance of crosswind responses and the crosswind acceleration exceeding comfort levels, discussions of controlled systems will primarily focus on crosswind responses.

5.2 TMD system

The performance of the TMD depends on its frequency and damping ratios. Fig. 7 illustrates the variation in normalized crosswind acceleration, defined as the ratio of the controlled structure's acceleration at the reference height to that of the uncontrolled structure, for different values of frequency and damping ratios. According to the figure, the optimal frequency and damping ratios that minimize the structural response are approximately 1.0 and 0.02, respectively. The precise optimal values for these parameters require an optimization technique.

The optimal design parameters for both the TMD and TMDI were determined through an iterative optimization process. The objective was to minimize crosswind acceleration at the

reference height. The optimization began with an initial guess based on theoretical relations for the optimum TMD parameters, derived from a two-degree-of-freedom (DOF) model by Warburton (1982), as follows:

$$f_{r_{opt}} = \frac{(1+\mu)^{1/2}}{1+\mu} \quad , \qquad \zeta_{r_{opt}} = \sqrt{\frac{\mu(1+3\mu/4)}{4(1+\mu)(1+\mu/2)}} \tag{28}$$

Where $f_{r_{opt}}$ and $\zeta_{r_{opt}}$ are the optimal frequency and damping ratios, respectively, and μ represents the mass ratio. To evaluate the vibration control efficiency of the TMD, the tower's responses at the reference height are computed for various TMD mass ratios (μ = 0% to 5%). For a TMD mass ratio of μ = 1%, the TMD mass is approximately 55.17 tons. Table 2 presents the results, including the TMD mass ratio, corresponding optimal TMD parameters, and the structure and TMD responses. The table shows that the structural response decreases with increasing μ. Notably, for μ = 0.5% and μ = 5%, the reductions in crosswind acceleration are 20.29% and 43.73%, respectively. A higher mass ratio (μ) improves vibration control by increasing the TMD's inertia, allowing it to more effectively counteract the building's motion and reduce wind-induced vibrations.

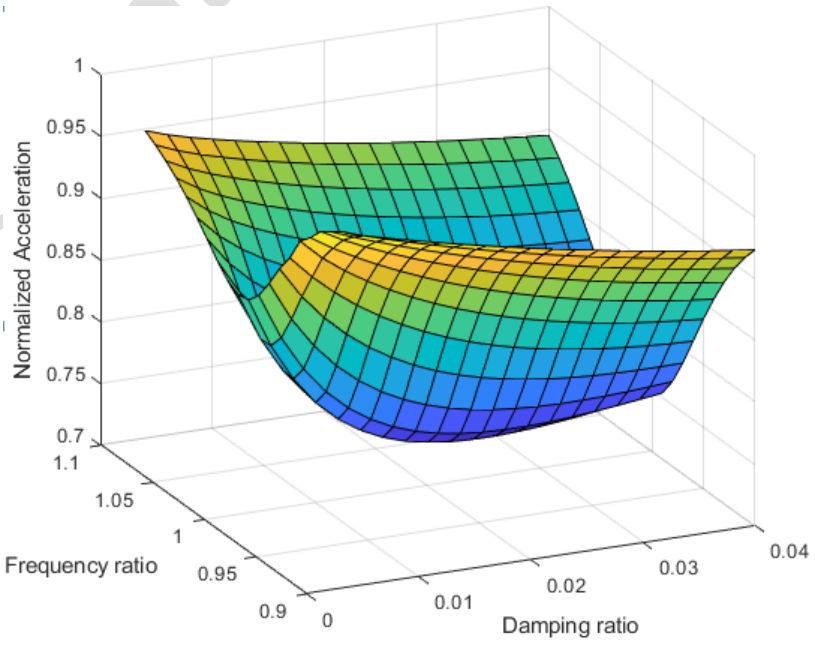

Fig. 7: Variation in normalized crosswind acceleration at the reference height as a function of frequency and damping ratios.

Table 2. TMD mass ratio and associated crosswind response values for the tower and TMD

Mass ratio μ (%)	Optimum parameters		Cross-wind responses		TMD response	Acceleration Reduction (%)
	$f_{d_{opt}}$	$\zeta_{d\,opt}$	σ_{x_c}(cm)	$\sigma_{\ddot{x}_c}$(cm/s^2)	σ_{x_cT}(cm)	
0			8.87	8.50		
0.5	1.0020	0.0176	6.93	6.77	125.53	20.29
1	1.0029	0.0248	6.29	6.21	84.18	26.88
2	1.0042	0.0352	5.60	5.61	54.92	34.02
3	1.0052	0.0431	5.18	5.24	42.30	38.31
4	1.0064	0.0498	4.88	4.98	34.99	41.37
5	1.0074	0.0558	4.64	4.78	30.11	43.73

5.3 TMDI system

To evaluate the vibration control efficiency of the TMDI, the responses of the structure are computed for μ=1%, and various values of height difference between the inerter terminals, Δh_i, and inertance ratio, β. Table 3 displays the structure and TMD responses for μ=1% and β=25%, considering different values of Δh_i. Fig. 8(a) shows the variation in crosswind acceleration reduction with respect to Δh_i for this scenario. The results indicate that, for constant mass and inertance ratios, the control efficiency of the TMDI improves with increasing Δh_i, because of the greater acceleration difference between the inerter terminals. Table 4 provides the responses for μ=1% and Δh_i=60m, with β varying between 0 and 40%. Fig. 8(b) shows how the reduction in crosswind acceleration changes with different values of β. For β=0%, the acceleration reduction is 26.88%. This reduction increases to 45.13% for β=40%.

Table 3. Crosswind responses for the tower and TMDI for μ=1% and β=25% as a function of Δh_i

Δh_i (m)	Optimum parameters		Cross-wind responses		TMDI response	Acceleration Reduction (%)
	$f_{d_{opt}}$	$\zeta_{d\,opt}$	σ_{x_c}(cm)	$\sigma_{\ddot{x}_c}$(cm/s^2)	σ_{x_cT}(cm)	

0	1.0029	0.025	6.29	6.21	84.18	26.88
30.0	1.0028	0.027	6.13	6.06	17.28	28.64
40.0	1.0040	0.034	5.67	5.66	17.19	33.40
50.0	1.0054	0.041	5.27	5.31	15.58	37.50
60.0	1.0068	0.048	4.94	5.03	14.57	40.80
80.0	1.0097	0.062	4.44	4.60	13.31	45.91

Table 4. Crosswind responses for the tower and TMDI for μ=1% and Δh_i=60m versus β

Inertance ratio β(%)	Optimum parameters		Cross-wind responses		TMDI response	Acceleration Reduction (%)
	$f_{d_{opt}}$	$\zeta_{d_{opt}}$	σ_{x_c}(cm)	$\sigma_{\ddot{x}_c}$(cm/s^2)	σ_{x_cT}(cm)	
0	1.0029	0.0248	6.29	6.21	84.18	26.88
5	1.0030	0.0281	6.05	5.99	33.91	29.50
10	1.0040	0.0341	5.66	5.65	24.15	33.48
20	1.0058	0.0441	5.13	5.20	16.55	38.85
30	1.0077	0.0523	4.78	4.89	13.12	42.45
40	1.0095	0.0597	4.52	4.66	11.09	45.13

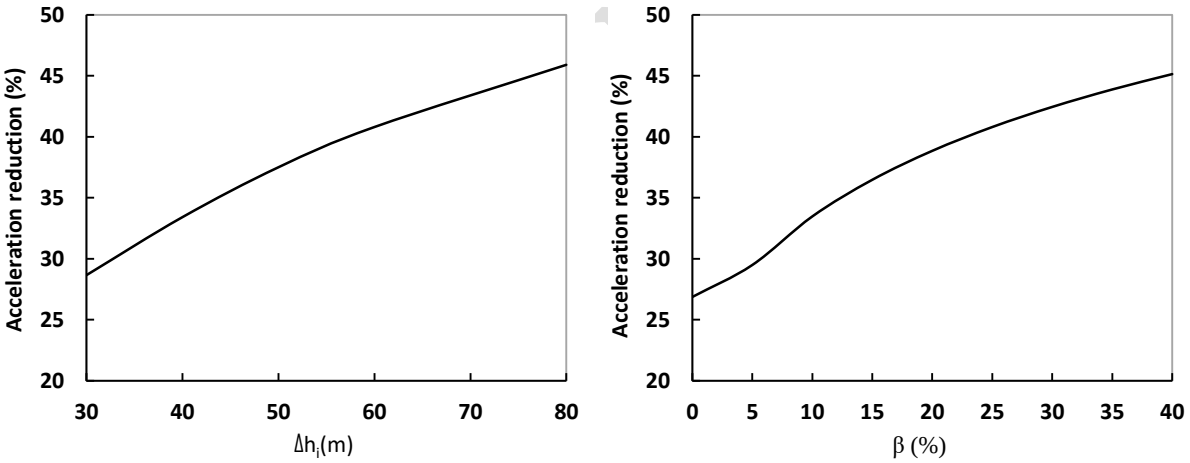

(a) (b)

Fig. 8. Crosswind acceleration reduction percentages for: (a) μ=1% and β=25% as a function of Δh_i , (b) μ=1% and Δh_i=60m for different values of β

5.4 ATMD system

To examine the effect of ATMD, the responses of the tower equipped with this system at the reference height for μ=1% are computed using the LQR technique for different values of the ratios q_1/q_2 and q_1/R, which are introduced in Section 3.3. Fig. 9 illustrates variations in

crosswind acceleration reduction for different values of q_1/q_2 and q_1/R ratios. The q_1/q_2 ratio ranges from 20 to 200, and the designated values for q_1/R are 10^9, 10^{10}, 10^{11}, and 10^{12}. As illustrated in this figure, the response of the structure decreases with an increase in q_1/q_2 and q_1/R ratios. Within the assumed range of values for these ratios, the maximum reduction in acceleration is 57.03%.

Fig. 10 shows the variation in RMS active force as a function of q_1/q_2 and q_1/R. As depicted, the active force shows an upward trend with increasing values of these ratios, reaching a maximum RMS active force of 28.97 kN within the assumed range of the ratios.

Fig. 11 illustrates the RMS displacement of the ATMD versus q_1/q_2 and q_1/R for μ=1%, demonstrating a distinctive response pattern compared to the structure. In contrast to the structural response, the ATMD system exhibits an increase in response with higher q_1/q_2 and q_1/R ratios. For instance, for q_1/q_2= 200 and q_1/R=1e12, which corresponds to the maximum control action, the RMS displacement of the ATMD is 158.16 cm, indicating that the displacement of the ATMD exceeds that of the TMD system by 88%. Therefore, it is crucial to note that the higher control performance of the ATMD on the main structure is directly associated with an increase in the ATMD's vibration amplitude.

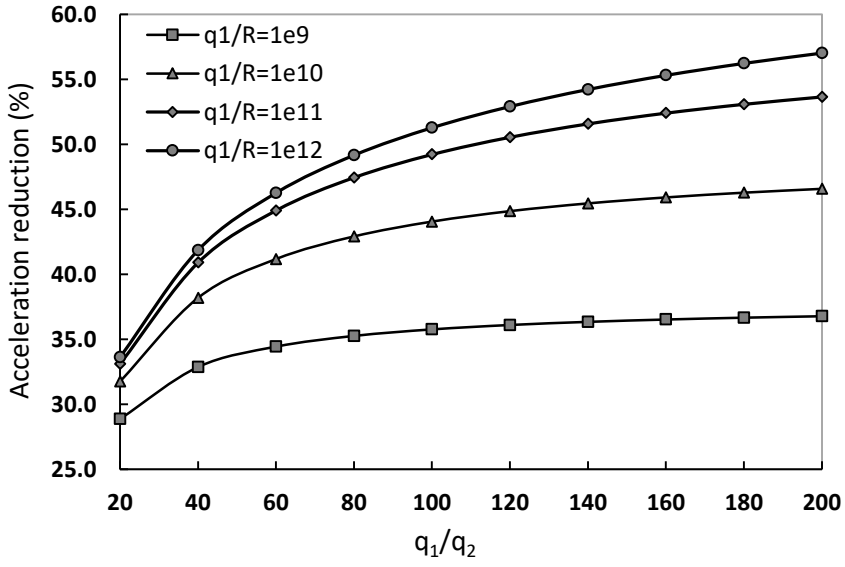

Fig. 9. Variation of crosswind acceleration reduction for the ATMD-equipped structure versus q_1/q_2 and q_1/R for μ=1%.

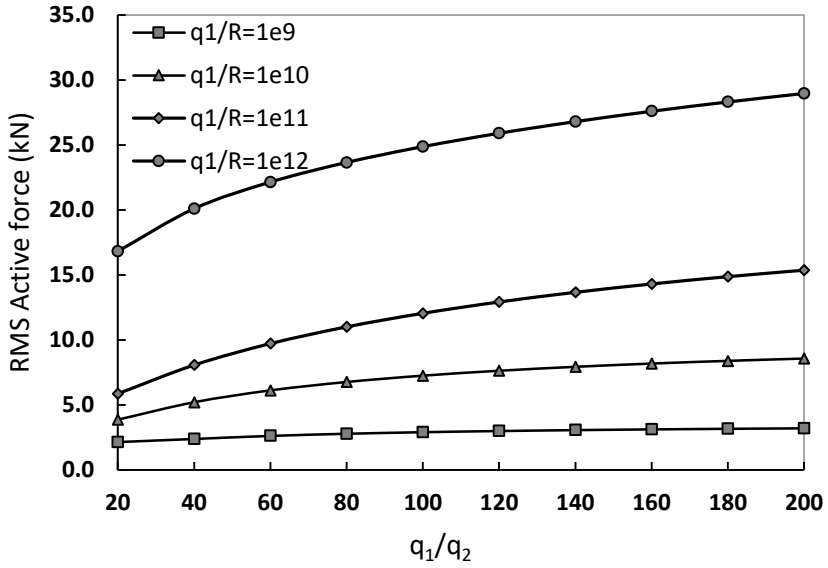

Fig. 10. Variation of RMS active force for the ATMD versus q_1/q_2 and q_1/R for μ=1%

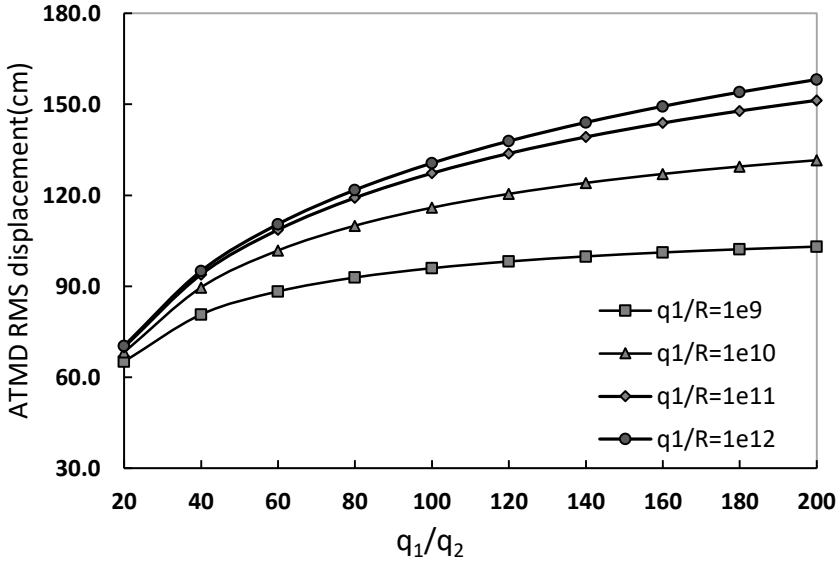

Fig. 11. RMS displacement of the ATMD as a function of q_1/q_2 and q_1/R for μ=1%

5.5 ATMDI system

For the ATMDI system, control efficiency depends on several factors. These include the mass ratio μ, the ratios q_1/q_2 and q_1/R, the inertance ratio β, which relates to the inerter's contribution to the system's overall inertia (Eq. (18)). Another important factor is the vertical

distance between the two terminals of the inerter Δh_i. A larger Δh_i results in a greater acceleration difference between the terminals, which subsequently increases the inerter force and improves the system's control performance.

Figures 12, 13, and 14 respectively show the variations in crosswind acceleration reduction, RMS active force, and RMS displacement of the ATMDI system for $\Delta h_i = 60\,m$, μ=1%, q_1/q_2=200, under different values of inertance and q1/R ratios. The curves corresponding to $\beta = 0$ represent the performance of the ATMD system. These figures indicate that the control effectiveness of the system improves with increasing values of β and q_1/R, which requires higher active force. On the other hand, as β increases, the displacement of the ATMDI system decreases, which is an advantage of this system.

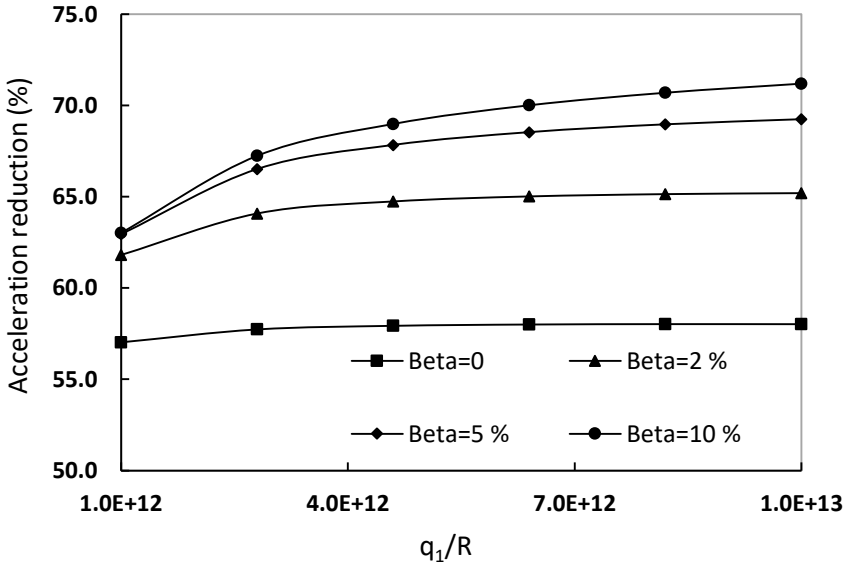

Fig. 12. Crosswind acceleration reduction for the ATMDI-equipped structure with $\Delta h_i = 60m$, μ=1%, q_1/q_2=200 versus β and q_1/R

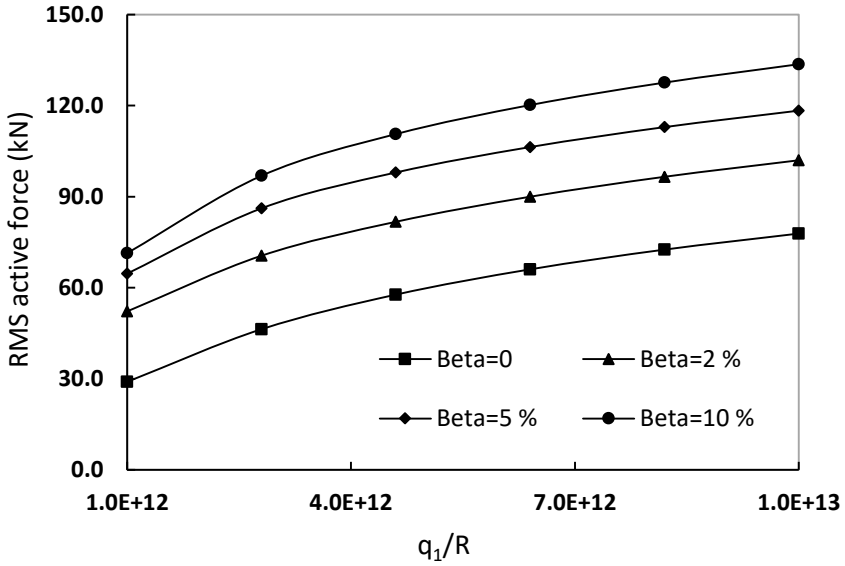

Fig. 13. Variation of RMS active force for the ATMDI-equipped structure with $\Delta h_i = 60\ m$, μ=1%, q_1/q_2=200 versus β and q_1/R

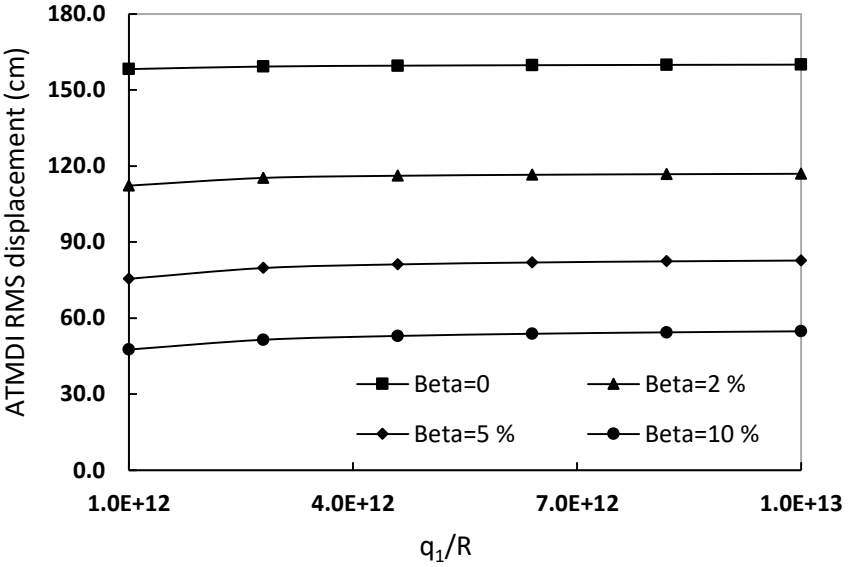

Fig. 14. RMS displacement of ATMDI for $\Delta h_i = 60m$, μ=1%, q_1/q_2=200 versus β and q_1/R

Table 5 presents the crosswind responses of the structure and the ATMDI for μ =1%, Δh_i =60 m, q_1/q_2=200, and q_1/R=5.0E12, with the inertance ratio varying from 0% to 10%. The

table demonstrates that the inerter significantly improves the control efficiency of the system, with higher values of β leading to more effective control actions. For instance, the acceleration reduction values for β = 0% and β = 10% are 57.96% and 69.18%, respectively.

Table 5. Crosswind responses of the tower equipped with ATMDI for μ=1%, Δh_i =60m, q_1/q_2=200 and q_1/R=5.0E12 versus β

Inertance ratio (β)	Cross-wind responses		ATMDI response	RMS Active force (kN)	Acceleration reduction (%)
	σ_{x_c}(cm)	$\sigma_{\ddot{x}_c}$(cm/s^2)	σ_{x_cT}(cm)		
0	3.260	3.572	159.59	59.76	57.96
2	2.564	2.989	116.27	83.82	64.82
4	2.288	2.774	90.62	95.81	67.35
6	2.164	2.683	73.69	104.18	68.42
8	2.103	2.640	61.80	109.91	68.93
10	2.072	2.619	53.05	113.92	69.18

Figures 15(a) and 15(b) illustrate the percentage reduction in crosswind acceleration and the ATMDI RMS displacement, respectively, as a function of β for mass ratios μ = 0.5% and μ =1%, with Δh_i = 60 m, q1/q2 = 200 and q_1/R=5.0E12. The figures indicate that as β increases, the difference between the responses for to the two mass ratios decreases, highlighting that the inerter plays a predominant role in vibration mitigation for the ATMDI systems examined. Additionally, as β increases, the system's stroke reduces. For instance, at β= 10%, the crosswind acceleration reduction is approximately 69%, and the ATMDI RMS displacement is about 53 cm. Thus, inclusion of the inerter in the ATMDI not only enhances the system's vibration mitigation effectiveness but also reduces its stroke compared to the ATMD.

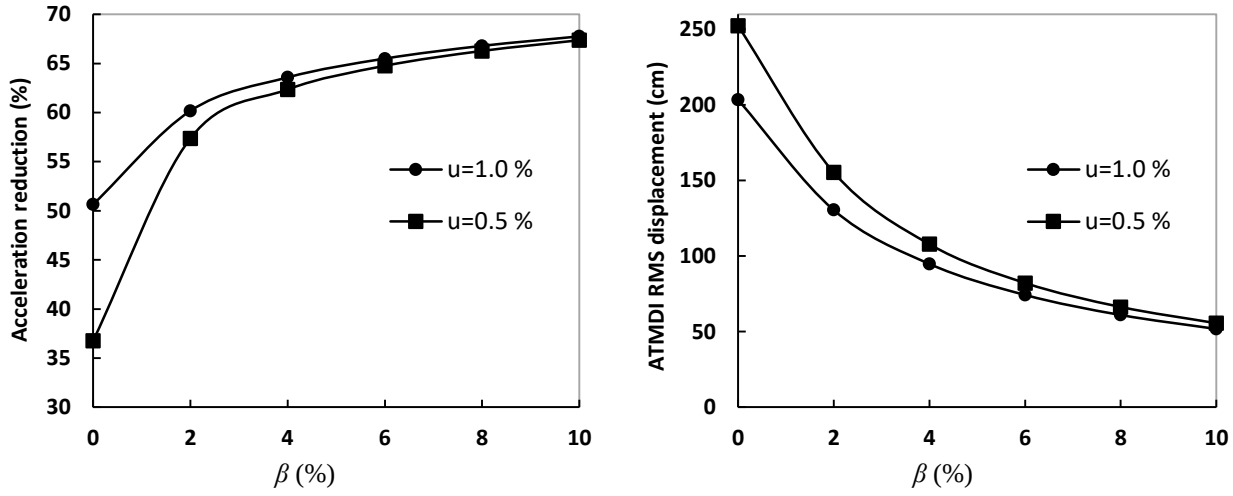

(a) (b)

Fig. 15: (a) Crosswind acceleration reduction percentages, and (b) ATMDI RMS displacement, for μ=0.5 and 1%, Δh_i=60m, q_1/q_2=200 and q_1/R=5.0E12 versus β

5.6 ATMDI Design Considerations

The numerical analysis in the preceding section evaluated ATMDI performance for the structure. Effective design of this hybrid control system requires establishing clear performance targets, typically defined by occupant comfort criteria where peak acceleration serves as the primary metric. As referenced in the introduction, acceptable acceleration thresholds for tall structures under a 10-year return period range from 15–20 cm/s² for offices to 10–15 cm/s² for residential buildings. For the case-study tower, the computed crosswind peak acceleration of 31.54 cm/s² exceeds these limits, requiring vibration control implementation.

The parametric study of an ATMDI configured with μ=1%, $\Delta h_i = 60\ m$, q_1/q_2=200, and $q_1/R=5.0\times10^{12}$ (Table 5) confirms the system's efficacy, demonstrating that its implementation across various inertance ratios yields acceleration reductions of 60–70%, thereby bringing structural responses within established comfort thresholds. This enhanced performance results from the combined action of the TMD, inerter, and active actuator, which together enable considerable design versatility.

This versatility offers practical advantages. For example, to achieve a specific design objective, such as a 62% acceleration reduction (corresponding to β=1% in Table 5), multiple

design alternatives exist. Table 6 presents various combinations of mass ratio (μ), inerter height difference (Δh_i), and inertance ratio (β) to achieve this control level, which allows designers to balance performance objectives against practical constraints such as the required space for the TMD mass block, the installation feasibility of the inerter mechanism, and the capacity and power requirements of the active actuator. Consequently, the design process becomes an optimization exercise within a multi-parameter solution space, enabling selection of the most feasible and efficient configuration for a given project.

Table 6. Alternative ATMDI designs for a sample 62% crosswind acceleration reduction target (q_1/q_2=200 and q_1/R=5.0E12)

Mass ratio μ(%)	height difference Δh_i(m)	Inertance ratio β(%)	RMS Active force (kN)
1.0	30	2.7	92.5
1.0	40	1.8	83.64
1.0	50	1.3	79.04
1.0	60	1.0	76.21
0.5	30	11.0	106.69
0.5	40	4.9	142.70

6. Conclusion

This study evaluated the effectiveness of the inerter-based active tuned mass damper (ATMDI) for controlling wind-induced vibrations in tall TV towers, and compared its performance with other systems, including TMD, TMDI, and ATMD. While the primary goal was to assess the ATMDI system, a parametric comparison of all four systems was also conducted. These comparative results provide valuable insights for selecting the most suitable system, customized for specific conditions and available resources in practical applications. A tall TV tower was modeled as a multi-degree-of-freedom system and structural responses were analyzed for basic wind speeds up to 30 m/s in both the crosswind and along-wind directions.

The maximum crosswind acceleration at a basic wind speed of 28 m/s was identified, which was approximately 93% greater than the maximum along-wind acceleration and surpassed the human comfort limits. Therefore, the effectiveness of the control systems in reducing crosswind acceleration is examined and discussed. Below is a summary of the results obtained under various conditions:

All four systems demonstrated a positive impact on reducing crosswind acceleration. However, the ATMDI system, which integrates both active control and the inerter, proved to be the most effective in vibration control. Specifically, the reductions in crosswind acceleration for μ=1% were 26.88% for TMD, 38.85% for TMDI ($\beta = 20\%$, Δh_i=60 m), 57.96% for ATMD (q_1/q_2=200 and q_1/R=5.0E12), and 69.18% for ATMDI ($\beta = 10\%$, Δh_i=60 m, q_1/q_2=200 and q_1/R=5.0E12).

Higher control efficiency for TMDs typically requires larger mass dampers, which can present installation challenges and may negatively impact internal forces in the structure, particularly seismic forces. The inerter enhances the performance of the mass damper without requiring a significantly large increase in mass. In the case of ATMD, the application of active force improves control, but the large stroke of the damper may limit its effectiveness. In contrast, the ATMDI system not only provides superior control but also significantly reduces the damper stroke compared to the ATMD.

Despite the advantages of the ATMDI system, its practical application comes with several limitations: 1) For a fixed mass ratio, the higher control capability of ATMDI compared to ATMD requires more active force; 2) In both TMDI and ATMDI systems, the performance of the inerter depends on the acceleration difference between its terminal attachment points, and in tall structures, the significant height difference required for effective inerter performance (e.g., more than 10% of the height of the reference point) may pose challenges for the

installation of the inerter; 3) The integration of the inerter with an active system introduces mechanical complexity, potentially leading to increased maintenance and operational costs.

Data Availability Statement

Some or all data, models, or code that support the findings of this study are available from the corresponding author upon reasonable request.

Acknowledgement

This work is based on research funded by Iran National Science Foundation (INSF) under project No.4014785. The author is grateful for the financial support from the INSF.

References

Aydin, E., Öztürk, B., Kebeli, Y.E., Gültepe, G. (2023). "An Experimental Study on the Effects of Different Pendulum Damper Designs on Structural Behavior", In: Cimellaro, G.P. (eds) Seismic Isolation, Energy Dissipation and Active Vibration Control of Structures. WCSI 2022. Lecture Notes in Civil Engineering, vol. 309. Springer, Cham, https://doi.org/10.1007/978-3-031-21187-4_18

Cetin, H., Aydin, E. and Ozturk, B. (2025). "Multiple Tuned Mass Damper Design for the Mitigation of Cantilever Beam Response", *ASCE-ASME Journal of Risk and Uncertainty in Engineering Systems, Part A: Civil Engineering*, 11(3), https://doi.org/10.1061/ajrua6.rueng-1502

Cetin, H., Kebeli, Y.E., Aydin, E., Ozturk, B., Ugu, B.A. (2025). "Experimental Evaluation of Tuned Mass Dampers for Seismic Vibration Control in Scaled Steel Structures", International Conference on Energy-Based Seismic Engineering (IWEBSE), In: Dindar, A.A., Benavent-Climent, A., Mollaioli, F., Varum, H. (eds) Energy-Based Seismic Engineering. Lecture Notes in Civil Engineering, vol 692. Springer, Cham, https://doi.org/10.1007/978-3-031-97129-7_29

Dai J., Xu Z.-D., & Gai, P.-P., (2019). "Tuned mass-damper-inerter control of wind-induced vibration of flexible structures based on inerter location", *Engineering Structures*, 199, 109585, https://doi.org/10.1016/j.engstruct.2019.109585

Dai, J., Xu, Z.-D., Gai, P.-P., & Hu, Z.-W, (2021). "Optimal design of tuned mass damper inerter with a Maxwell element for mitigating the vortex-induced vibration in

bridges", *Mechanical Systems and Signal Processing*, 148, 107180, https://doi.org/10.1016/j.ymssp.2020.107180

De Angelis, M., Basili, M., & Pietrosanti, D., (2023). "On the optimal design and placement of Tuned-Mass-Damper-Inerter for Multi-Degree-Of-Freedom structures", *Structures*, 56, 104781, https://doi.org/10.1016/j.istruc.2023.06.112

Elias, S., Matsagar, V., & Datta, T. K., (2019). "Along-wind response control of chimneys with distributed multiple tuned mass dampers", *Structural Control and Health Monitoring*, 26(1), e2275, https://doi.org/10.1002/stc.2275

Giaralis A., Petrini F., (2017a). "Optimum design of the tuned mass-damper-inerter for serviceability limit state performance in wind excited tall buildings", *Procedia Engineering*, 199, 1773–1778, https://doi.org/10.1016/j.proeng.2017.09.453

Giaralis A., Petrini F., (2017b). "Wind-induced vibration mitigation in tall buildings using the tuned mass-damper-inerter (TMDI)", *Journal of Structural Engineering*, 143, 4017127, https://doi.org/10.1061/(asce)st.1943-541x.0001863

He, Y. C., & Li, Q., (2014). "Dynamic responses of a 492-m-high tall building with active tuned mass damping system during a typhoon", *Structural Control and Health Monitoring*, 21(5), 705-720, https://doi.org/10.1002/stc.1596

Jafari, M., & Alipour, A., (2021). "Methodologies to mitigate wind-induced vibration of tall buildings: A state-of-the-art review", *Journal of Building Engineering*, 33, 101582, https://doi.org/10.1016/j.jobe.2020.101582

Johann, F. A., Carlos, M. E. N., & Ricardo, F. L. S., (2015). "Wind-induced motion on tall buildings: A comfort criteria overview", *Journal of Wind Engineering and Industrial Aerodynamics*, 142, 26–42, https://doi.org/10.1016/j.jweia.2015.03.001

Khodaie, N., (2020). "Vibration control of super-tall buildings using combination of tapering method and TMD system", *Journal of Wind Engineering and Industrial Aerodynamics*, 196, 104031, https://doi.org/10.1016/j.jweia.2019.104031

Khodaie, N., Eimani, H., (2018). "Wind-induced vibration control of tall TV towers using a part of the main structure as a vibration absorber substructure", *Journal of structural and construction engineering*, 6(2), 109-126, https://doi.org/10.22065/jsce.2018.95021.1285

Kim, Y. M., You, K. P., & You, J. Y., (2014). "Active control of along-wind response of a tall building with AMD using LQR controller", *Applied Mechanics and Materials*, 490–491, 1063–1067, https://doi.org/10.4028/www.scientific.net/amm.490-491.1063

Kwon, D. K., Kareem, A., (2013). "Comparative study of major international wind codes and standards for wind effects on tall buildings", *Engineering Structures*, 51. 23–35, https://doi.org/10.1016/j.engstruct.2013.01.008

Lara-Valencia L. A., Farbiarz-Farbiarz Y., & Valencia-González Y., (2020). "Design of a Tuned Mass Damper Inerter (TMDI) Based on an Exhaustive Search Optimization for Structural Control of Buildings under Seismic Excitations", *Shock and Vibration*, 8875268, https://doi.org/10.1155/2020/8875268

Lazar I.F., Neild S.A., and Wagg D.J., (2014). "Using an inerter-based device for structural vibration suppression", *Earthquake Engineering & Structural Dynamics*, 43: 1129-1147, https://doi.org/10.1002/eqe.2390

Liang R., Wang H., Li J., Gao H., Zheng W., & Xu Z., (2021). "Multiple tuned inerter-based dampers for seismic response mitigation of continuous girder bridges", *Soil Dynamics and Earthquake Engineering*, 151, 106954, https://doi.org/10.1016/j.soildyn.2021.106954

Li, C., (2002). "Optimum multiple tuned mass dampers for structures under the ground acceleration based on DDMF and ADMF", *Earthquake Engineering & Structural Dynamics*, 31(4), 897-919, https://doi.org/10.1002/eqe.128.abs

Li, L., Song, G., Ou, J., (2011). "Hybrid active mass damper (AMD) vibration suppression of nonlinear high-rise structure using fuzzy logic control algorithm under earthquake excitations", *Structural Control and Health Monitoring*, 18, 698–709, https://doi.org/10.1002/stc.402

Ma R., Bi K., & Hao H., (2021). "Inerter-based structural vibration control: A state-of-the-art review", *Engineering Structures*, 243, 112655, https://doi.org/10.1016/j.engstruct.2021.112655

Mei, Z., Guo, Z., Chen, L., Wang, H. and Gao, Y., (2020). "Genetic algorithm-based integrated optimization of active control systems for civil structures subjected to random seismic excitations", *Engineering Optimization*, 52(10), 1700-1719, https://doi.org/10.1080/0305215x.2019.1677632

Menon, D., & Rao, P. S., (1997). "Uncertainties in codal recommendations for across-wind load analysis of R/C chimneys", *Journal of Wind Engineering and Industrial Aerodynamics*, 72, 455–468, https://doi.org/10.1016/s0167-6105(97)00267-5

Najafi, S., Aghayari, R., Cheraghi, K. and TahamouliRoudsari, M. (2024). "Experimental and numerical study of the effect of friction damper on the seismic behavior of concrete frame", *Civil Engineering Infrastructures Journal*, https://doi.org/10.22059/ceij.2024.378792.2088

NBCC, (2010). National building code of Canada, Associate Committee on the National Building Code, National Research Council.

Pandey D. K., & Mishra S. K., (2021). "Inerter assisted robustness of compliant liquid column damper, Structural Control and Health Monitoring", 28(8), e2763, https://doi.org/10.1002/stc.2763

Peng, Y., & Sun, P., (2024). "Reliability-based design optimization of tuned mass-damper-inerter for mitigating structural vibration", *Journal of Sound and Vibration*, 572, 118166, https://doi.org/10.1016/j.jsv.2023.118166

Pinkaew T., Fujino Y., (2001). "Effectiveness of semi-active tuned mass dampers under

harmonic excitation", *Engineering Structures*, 23, 850–856, https://doi.org/10.1016/s0141-0296(00)00091-2

Qiao, H., Huang, P., De Domenico, D., & Wang, Q., (2022). "Structural control of high-rise buildings subjected to multi-hazard excitations using inerter-based vibration absorbers", *Engineering Structures*, 266, 114666, https://doi.org/10.1016/j.engstruct.2022.114666

Ricciardelli, F., Pizzimenti, A.D. and Mattei, M., (2003). "Passive and active mass damper control of the response of tall buildings to wind gustiness", *Engineering Structures*, 25(9), 1199-1209, https://doi.org/10.1016/s0141-0296(03)00068-3

Shahi, M., Sohrabi, M. R., & Etedali, S., (2018). "Seismic Control of High-Rise Buildings Equipped with ATMD Including Soil-Structure Interaction Effects", *Journal of Earthquake and Tsunami*, 12(03), 1850010, https://doi.org/doi/10.1142/S1793431118500100

Simiu, P.E., (2011). "Design of buildings for wind, A Guide for ASCE 7-10 Standard users and designers of special structures", Second Edition, John Wiley & Sons INC., Hoboken, New Jersey.

Simiu, P.E., Yeo, D., (2019). "Wind effects on structures: modern structural design for wind", 4th edition, John Wiley & Sons Ltd.

Smith M.C., (2002). "Synthesis of mechanical networks: the inerter", *IEEE Transactions on Automatic Control*, 47:1648–62, https://doi.org/10.1109/cdc.2002.1184758

Su, N., Peng, S., Hong, N., & Xia, Y., (2022). "Wind-induced vibration absorption using inerter-based double tuned mass dampers on slender structures", *Journal of Building Engineering*, 58, 104993, https://doi.org/10.1016/j.jobe.2022.104993

Sun L., Hong D., & Chen L., (2017). "Cables interconnected with tuned inerter damper for vibration mitigation", *Engineering Structures*, 151, 57–67, https://doi.org/10.1016/j.engstruct.2017.08.009

Suthar, S. J., (2024). "Response control of SDOF system with inerter-assisted tuned liquid sloshing damper", *Journal of Engineering Mechanics*, 150(8), 04024043, https://doi.org/10.1061/jenmdt.emeng-7618

Suthar, S. J., Banerji, P., (2023). "Inerter-assisted pendulum-tuned mass damper for across-wind response control of tall buildings", *Engineering Structures*, 291, 116489, https://doi.org/10.1016/j.engstruct.2023.116489

Suthar, S. J., Jangid, R. S., (2021). "Design of tuned liquid sloshing dampers using nonlinear constraint optimization for across-wind response control of benchmark tall building", *Structures*, 33, 2675-2688, https://doi.org/10.1016/j.istruc.2021.05.059

Ubertini, F., Comodini, F., Fulco, A., Mezzi, M., (2017). "A Simplified Parametric Study on Occupant Comfort Conditions in Base Isolated Buildings under Wind Loading", *Advances in Civil Engineering*, 2017, 3524975, 13 pages, https://doi.org/10.1155/2017/3524975

Wang Q., Tiwari N. D., Qiao H., & Wang Q., (2020). "Inerter-based tuned liquid column damper for seismic vibration control of a single-degree-of-freedom structure", *International Journal of Mechanical Sciences*, 184, 105840, https://doi.org/10.1016/j.ijmecsci.2020.105840

Wani, Z. R., Tantray, M., Noroozinejad Farsangi, E., Nikitas, N., Noori, M., Samali, B., & Yang, T. Y., (2022). "A Critical Review on Control Strategies for Structural Vibration Control", *Annual Reviews in Control*, 54, 103–124, https://doi.org/10.1016/j.arcontrol.2022.09.002

Weber F., Borchsenius F., Distl J., and Braun C., (2022), "Performance of Numerically Optimized Tuned Mass Damper with Inerter (TMDI)", *Applied Sciences*, 12, 6204, https://doi.org/10.3390/app12126204

Wu X., Liu X., Chen J., Liu K., Pang C., (2022). "Parameter Optimization and Application for the Inerter-Based Tuned Type Dynamic Vibration Absorbers", *Buildings*, 12(6), 703, https://doi.org/ 10.3390/buildings12060703

Xu, K., Bi, K., Han, Q., Li, X., & Du, X., (2019). "Using tuned mass damper inerter to mitigate vortex-induced vibration of long-span bridges: Analytical study", Engineering Structures, 182, 101–111, https://doi.org/10.1016/j.engstruct.2018.12.067

Yang, F., Sedaghati, R., Esmailzadeh, E., (2021). "Vibration suppression of structures using tuned mass damper technology: A state-of-the-art review", *Journal of Vibration and Control*, 0, 1077546320984305, https://doi.org/10.1177/1077546320984305

Zhang Z., Fitzgerald, B., (2022). "Tuned mass-damper-inerter (TMDI) for suppressing edgewise vibrations of wind turbine blades", *Engineering Structures*, 221, 110928, https://doi.org/10.1016/j.engstruct.2020.110928

Zhang, Z., Li, A., He, J. and Wang J., (2009). "Wind-induced vibration control of Hefei TV tower with fluid viscous damper", *Frontiers of Architecture and Civil Engineering in China*, 3, 249–254. https://doi.org/10.1007/s11709-009-0038-x

Zhou, K., Li, Q.-S., Li, X., (2020), "Dynamic Behavior of Supertall Building with Active Control System during Super Typhoon Mangkhut", *Journal of Structural Engineering*, 146, 04020077, https://doi.org/10.1061/(asce)st.1943-541x.0002626